Variation after projection with a triaxially deformed nuclear mean field

Zao-Chun Gao,[1,2,*] Mihai Horoi,[3] and Y. S. Chen[1]
[1]*China Institute of Atomic Energy, Beijing 102413, China*
[2]*State Key Laboratory of Theoretical Physics, Institute of Theoretical Physics, Chinese Academy of Sciences, Beijing 100190, China*
[3]*Department of Physics, Central Michigan University, Mount Pleasant, Michigan 48859, USA*
(Received 10 September 2015; revised manuscript received 12 November 2015; published 14 December 2015)

We implemented a variation after projection (VAP) algorithm based on a triaxially deformed Hartree-Fock-Bogoliubov vacuum state. This is the first projected mean field study that includes all the quantum numbers (except parity), i.e., spin (J), isospin (T), and mass number (A). Systematic VAP calculations with JTA projection have been performed for the even-even sd-shell nuclei with the USDB Hamiltonian. All the VAP ground state energies are within 500 keV above the exact shell model values. Our VAP calculations show that the spin projection has two important effects: (1) the spin projection is crucial in achieving good approximation of the full shell model calculation; (2) the intrinsic shapes of the VAP wave functions with spin projection are always triaxial, while the Hartree-Fock-Bogoliubov methods likely provide axial intrinsic shapes. Finally, our analysis suggests that one may not be possible to associate an intrinsic shape to an exact shell model wave function.

DOI: 10.1103/PhysRevC.92.064310 PACS number(s): 21.60.Jz, 21.60.Cs, 21.10.Hw

I. INTRODUCTION

The Hartree-Fock-Bogoliubov (HFB) method has been very successful in describing the global properties of the ground states throughout the whole nuclear region. As a mean field method, HFB breaks the symmetries of the nuclear system, and can be used to study the intrinsic shapes. The HFB calculations with Gogny force show that almost all the calculated 1712 nuclei have axially symmetric HFB minima [1].

Projection can be done on a HFB vacuum to recover the symmetries that the Hamiltonian obeys. To test the quality of the projected wave functions, one can compare them with the exact shell model ones using a common Hamiltonian. HFB and variation after projected HFB calculations with shell model Hamiltonians have been reported by several authors [2–5]. For those calculations without projection, the HFB vacuum states are often assumed to be axially symmetric [4]. Indeed, we will see below that all the calculated HFB minima in sd-shell nuclei, except ^{24}Mg, are exactly axial with the USDB Hamiltonian [6].

However, if one performs the variation of the projected HFB vacuum, usually called variation after projection (VAP) [7], it is likely that the intrinsic shape may change due to the inclusion of beyond mean field correlations. One typical example is the ground state (g.s.) of ^{32}Mg, which is predicted to be spherical at the mean field level [8], but it turns out to have a quadrupole deformation when the correlations associated with the restoration of the broken rotational symmetry are considered [9]. Another example is ^{56}Ni, whose ground state is spherical at the mean field level, but is slightly deformed when performing the projected energy surface calculation [10].

Moreover, the triaxial (γ) degree of freedom plays important roles on the low-lying collective dynamics in this mass region [12]. In ^{24}Mg the possibility of the triaxial deformation in the ground state was discussed for decades [13–15], and it is still being used as the testing ground for modern theories involving angular momentum (spin) projection [16–18].

In this work, we perform VAP calculations of the even-even sd-shell nuclei using the USDB Hamiltonian. Here, we allow the γ degree of freedom in the HFB transformation. The shell model Hamiltonian conserves the spin (J), isospin (T), as well as the mass number (A). Hence a complete projection should recover all J, T, and A quantum numbers. This is generally very time-consuming because of the seven-dimensional integration (three for J, three for T, and one for A). Presently, we can only carry out such extensive studies in the sd shell. For efficiency, we use the new techniques of Refs. [19–21] to evaluate the kernels for projections.

II. THE VAP METHOD

From a randomly chosen HFB vacuum state $|\Phi_0\rangle$, one can construct a new HFB vacuum state $|\Phi\rangle$ using the Thouless theorem [7]. Namely,

$$|\Phi\rangle = \mathcal{N} e^{\frac{1}{2}\sum_{\mu\nu} d_{\mu\nu} a_\mu^\dagger a_\nu^\dagger} |\Phi_0\rangle, \tag{1}$$

where d is a skew symmetric matrix, and $\mathcal{N}$ is the normalization factor. The triaxiality of the HFB vacuum can be treated similar to Ref. [22] so that the $Q_{2\pm1}$ components of the quadrupole moment vanish.

Projecting $|\Phi\rangle$ onto good quantum numbers J, T, and A, one gets the so-called JTA projection (similarly, TA projection for T, A, etc.). The JTA-projected wave function can be written as

$$|\Psi_{\mathrm{JTA},MM_T}\rangle = \sum_{KK_T} f_{KK_T} P^J_{MK} P^T_{M_T K_T} P^A |\Phi\rangle, \tag{2}$$

where P^J_{MK}, $P^T_{M_T K_T}$, and P^A are the spin, isospin, and mass number projection operators, respectively. The isospin projection operator is similar to the spin projection operator but in the isospin space. The corresponding JTA-projected energy is

$$E_{\mathrm{JTA}} = \langle \Psi_{\mathrm{JTA},MM_T} | \hat{H} | \Psi_{\mathrm{JTA},MM_T} \rangle = \sum_{K'KK'_TK_T} f^*_{K'K'_T} f_{KK_T} \langle \Phi | \hat{H} P^J_{K'K} P^T_{K'_T K_T} P^A | \Phi \rangle. \tag{3}$$

*zcgao@ciae.ac.cn

$E_{\rm JTA}$ and the corresponding coefficients f_{KK_T} are obtained by solving

$$\sum_{KK_T}\langle\Phi|(\hat{H}-E_{\rm JTA})P^J_{K'K}P^T_{K'_TK_T}P^A|\Phi\rangle f_{KK_T}=0 \quad (4)$$

with f_{KK_T} satisfying

$$\sum_{K'KK'_TK_T} f^*_{K'K'_T}f_{KK_T}\langle\Phi|P^J_{K'K}P^T_{K'_TK_T}P^A|\Phi\rangle=1. \quad (5)$$

One can also perform the TA projection by simply removing the spin projection from Eqs. (2)–(5),

$$|\Psi_{{\rm TA},M_T}\rangle=\sum_{K_T}f_{K_T}P^T_{M_TK_T}P^A|\Phi\rangle, \quad (6)$$

$$\begin{aligned}E_{\rm TA}&=\langle\Psi_{{\rm TA},M_T}|\hat{H}|\Psi_{{\rm TA},M_T}\rangle\\&=\sum_{K'_TK_T}f^*_{K'_T}f_{K_T}\langle\Phi|\hat{H}P^T_{K'_TK_T}P^A|\Phi\rangle.\end{aligned} \quad (7)$$

For the A projection, the corresponding energy, E_A, is reduced to

$$E_A=\frac{\langle\Phi|\hat{H}P^A|\Phi\rangle}{\langle\Phi|P^A|\Phi\rangle}. \quad (8)$$

Without any projection, we define

$$E_{\rm HFB}=\langle\Phi|\hat{H}|\Phi\rangle. \quad (9)$$

It is natural that one may consider the neutron (N) and proton (Z) projection, as has been done in Refs. [2,5]. However, this is essentially the same as the M_TA projection [$M_T=(N-Z)/2$]. Here, we prefer to take the TA projection to recover the total isospin symmetry. In our case, the M_T projection is no longer necessary because the total isospin and the mass number are good quantum numbers. Thus all quantum numbers J, T ,N, and Z (parity is automatically good in the sd valence space) have been recovered in the present work. The sd valence space wave functions have the center of mass in its g.s., provided that harmonic oscillator single particle wave functions are considered.

VAP calculations can be performed by changing the d matrix in Eq. (1). Here, we impose the following restrictions for the d matrix: (1) d is real, (2) keeping the time reversal symmetry, and (3) no mixing between neutron and proton in the HFB transformation. Therefore the total number of free VAP parameters for the sd shell is reduced to $N_{\rm VAP}=42$. In practice we start with $d=0$ and with Nilsson+BCS vacuum states $|\Phi_0\rangle$ obtained with randomly chosen quadrupole parameters [10]. The triaxial degree of freedom is also allowed in $|\Phi_0\rangle$.

We follow the VAP algorithm whose details were introduced in Ref. [5]. Here are the main steps used in our VAP calculations. Given a certain d matrix, one can get the corresponding HFB transformation for the vacuum $|\Phi\rangle$ [5]. Solving Eq. (4), one can obtain several $E_{\rm JTA}$ eigenenergies for the single $|\Phi\rangle$. The lowest $E_{\rm JTA}$ and the corresponding coefficients f_{KK_T} are considered. Having fixed all f_{KK_T}, one can evaluate the partial derivatives $\frac{\partial E_{\rm JTA}}{\partial d_{\mu\nu}}$ whose expression can be obtained from Eq. (3) [5]. If $E_{\rm JTA}$ reaches a minimum, then $\frac{\partial E_{\rm JTA}}{\partial d_{\mu\nu}}\approx 0$ for all selected $d_{\mu\nu}$ parameters and the VAP calculation terminates. Otherwise, we continue to search for a minimum using a gradient method [11] that updates the d matrix and is going to the next iteration.

To extract the intrinsic shape, the quadrupole moment and the triaxial degree of freedom, Q and γ, are defined such that

$$Q\cos\gamma=\langle\Psi|\sqrt{\frac{16\pi}{5}}\frac{r^2}{b^2}Y_{20}|\Psi\rangle, \quad (10)$$

$$Q\sin\gamma=\langle\Psi|\sqrt{\frac{16\pi}{5}}\frac{r^2}{b^2}\frac{1}{\sqrt{2}}(Y_{22}+Y_{2-2})|\Psi\rangle, \quad (11)$$

where b is the harmonic oscillator length. $|\Psi\rangle$ refers to an intrinsic state, which may have different forms. Explicitly, we define

(1) $Q_{\rm HFB}$ and $\gamma_{\rm HFB}$ for $|\Psi\rangle=|\Phi\rangle$,
(2) Q_A and γ_A for $|\Psi\rangle=\frac{P^A|\Phi\rangle}{\sqrt{\langle\Phi|P^A|\Phi\rangle}}$, and
(3) $Q_{\rm TA}$ and $\gamma_{\rm TA}$ for $|\Psi\rangle=|\Psi_{{\rm TA},M_T}\rangle$.

III. VAP CALCULATIONS FOR ^{24}Mg

When performing the energy variation, one may find that there might be more than one energy minima. Therefore, the energy variation should be calculated several times with different starting $|\Phi_0\rangle$ states which are randomly chosen. We then identify the lowest minimum, and denote it with E^*. Here and below, we only discuss the results corresponding to E^*.

In the present work, we adopt the USDB Hamiltonian [6]. The HFB energy for ^{24}Mg is $E^*_{\rm HFB}=-80.965$ MeV with the constraints $\langle\Phi|\hat{N}|\Phi\rangle=N$ and $\langle\Phi|\hat{Z}|\Phi\rangle=Z$. This is the only sd-shell nucleus for which the HFB calculation gives a nonaxial shape with $Q^*_{\rm HFB}=18.659$ and $\gamma^*_{\rm HFB}=11.96^\circ$ (here and below the Q^* and γ^* are the shape parameters that can be associated with the absolute minimum for some VAP choice). Let us first do the simplest VAP with only

TABLE I. Results of the VAP-A calculations for ^{24}Mg. We perform the VAP calculations for several times. Each time we start with different $|\Phi_0\rangle$ states. The numbers in the first column denote different $|\Phi_0\rangle$ states. The second column shows the converged energy E^*_A. Quantities in other columns are calculated with the converged $|\Phi\rangle$ vacua. Energies are in MeV.

$\lvert\Phi_0\rangle$	E^*_A	Q_A	$\gamma_A(^\circ)$	$E_{\rm HFB}$	$Q_{\rm HFB}$	$\gamma_{\rm HFB}(^\circ)$	$\langle\hat{A}\rangle$
1	−81.358	18.284	10.05	−81.008	18.005	9.46	8.110
2	−81.358	18.284	130.05	−90.178	18.371	128.94	9.013
3	−81.358	18.284	−109.95	−82.684	18.120	−110.61	8.259
4	−81.358	18.284	10.05	−79.720	17.905	9.05	8.000

TABLE II. Similar to Table I but for the VAP-TA calculations. $\langle A\rangle = 8$ is imposed.

$\|\Phi_0\rangle$	$E^*_{\rm TA}$(MeV)	$Q_{\rm TA}$	$\gamma_{\rm TA}(^\circ)$	E_A(MeV)	Q_A	$\gamma_A(^\circ)$	$E_{\rm HFB}$(MeV)	$Q_{\rm HFB}$	$\gamma_{\rm HFB}(^\circ)$	$\langle A\rangle$
1	−82.831	17.295	−119.91	−75.826	16.376	−118.62	−74.921	15.755	−118.23	8.000
2	−82.831	17.295	0.09	−74.402	16.167	2.47	−73.909	15.563	3.06	8.000
3	−82.831	17.295	120.09	−76.633	16.526	120.09	−75.525	15.897	120.08	8.000

A projection (called VAP-A). Since the particle number is already projected out, it might be unnecessary to impose a constraint to the average particle number of the HFB vacuum. To check this conjecture, we start from several different $|\Phi_0\rangle$ states and perform VAP-A. The results for few selected $|\Phi_0\rangle$ choices are shown in Table I. One can see that the VAP-A energies are identical ($E^*_A = -81.358$ MeV). However, the corresponding $E_{\rm HFB}$, $Q_{\rm HFB}$, $\gamma_{\rm HFB}$, and $\langle\hat{A}\rangle \equiv \langle\Phi|\hat{A}|\Phi\rangle$ appear randomly, but after the A projection, the Q_A values are the same. Although the γ_A values look different, the numbers indicate the same shape but with different orientations. All these results imply that although the converged vacua $|\Phi\rangle$ are not unique, they correspond to the same A-projected state. This can be further confirmed by calculating the overlaps between these projected states corresponding to different $|\Phi\rangle$. Our calculations show that all these overlaps among the converged HFB vacua in Table I are found to be 1 except for an arbitrary phase, i.e.,

$$\frac{\langle\Phi|P^A|\Phi'\rangle}{\sqrt{\langle\Phi|P^A|\Phi\rangle\langle\Phi'|P^A|\Phi'\rangle}} = e^{i\delta}, \tag{12}$$

where δ is a real number. $|\Phi\rangle$ and $|\Phi'\rangle$ are different converged HFB vacua, but $|\Phi'\rangle$ is the reoriented one whose γ_A value should be the same as for $|\Phi\rangle$.

Therefore, one can adopt the values $Q^*_A = 18.284$ and $\gamma^*_A = 10.05$ to define the shape of the VAP-A minimum. If one imposes $\langle\hat{A}\rangle = A = 8$, we still have $E^*_A = -81.358$ MeV, now the converged $|\Phi\rangle$ vacuum becomes unique, with $E_{\rm HFB} = -79.720$, $Q_{\rm HFB} = 17.905$, and $\gamma_{\rm HFB} = 9.05^\circ$ (see the last line in Table I). However, for the VAP with TA projection, the situation becomes a little different.

VAP calculations with TA projection (called VAP-TA) are listed in Table II. Unlike VAP-A, even if one imposes $\langle\hat{A}\rangle = A = 8$ for ^{24}Mg, the converged $|\Phi\rangle$ is still not unique as the $E_{\rm HFB}$ energy appears randomly. Moreover, the E_A energy is not unique either. Interestingly, after TA projection, those different $|\Phi\rangle$ vacuum states have exactly the same projected energy $E^*_{\rm TA} = -82.831$(MeV) and the same $Q^*_{\rm TA} = 17.295$. Similarly, we found (after rotation) $\gamma^*_{\rm TA} = 0.09^\circ$, which describes an almost axial shape. Again, our calculations show that the overlaps of the TA-projected states satisfy

$$\langle\Psi_{{\rm TA},M_T}|\Psi'_{{\rm TA},M_T}\rangle = \sum_{K_T K'_T} f^*_{K_T} f'_{K'_T} \langle\Phi|P^T_{K_T K'_T} P^A|\Phi'\rangle = e^{i\delta}, \tag{13}$$

where $|\Phi'\rangle$ generating $|\Psi'_{{\rm TA},M_T}\rangle$ should be treated similar to that in Eq. (12). One can conclude that those VAP-TA projected states in Table II are essentially identical and the associated shape can only be described by $Q_{\rm TA}$ and $\gamma_{\rm TA}$.

A complete symmetry restoration is the JTA projection. VAP results with JTA projection (called VAP-JTA) are shown in Table III. All the converged $E^*_{\rm JTA}$ energies are −86.919 MeV, significantly closer to the shell model result $E_{\rm SM} = -87.105$ MeV. Overlap calculations clearly confirm that those JTA-projected states are identical, i.e.,

$$\begin{aligned}\langle\Psi_{{\rm JTA},MM_T}|\Psi'_{{\rm JTA},MM_T}\rangle &= \sum_{KK_TK'K'_T} f^*_{KK_T} f'_{K'K'_T} \langle\Phi|P^J_{KK'} P^T_{K_TK'_T} P^A|\Phi'\rangle \\ &= e^{i\delta}.\end{aligned} \tag{14}$$

Here, $|\Phi'\rangle$ does not need to be reoriented due to the inclusion of the spin projection.

Again, both E_A and $E_{\rm HFB}$ in Table III cannot be uniquely determined, even if one enforces the $\langle\hat{A}\rangle = A$ constraint. Fortunately, with the additional spin projection, all $E_{\rm TA}$ values are found to be −79.879 MeV, and similarly the corresponding shape is described by $Q_{\rm TA} = 19.057$ and $\gamma_{\rm TA} = 16.96^\circ$. Therefore, the quantities that can be associated with the shape of the VAP-JTA wave function should be $Q^*_{\rm TA} = 19.057$ and $\gamma^*_{\rm TA} = 16.96^\circ$.

One can study the shape evolution of ^{24}Mg from HFB to VAP-JTA. In VAP-TA, $Q^*_{\rm TA}$ looks smaller than $Q^*_{\rm HFB}$ in HFB, and $\gamma^*_{\rm TA}$ tends to be close to zero (axial shape). However in VAP-JTA, $Q^*_{\rm TA}$ is larger than the $Q^*_{\rm HFB}$ in HFB, and $\gamma^*_{\rm TA}$ tends to describe a triaxial shape. This triaxiality in VAP-JTA, in comparison with VAP-TA, is likely caused by the spin projection. Nuclear triaxiality caused by the spin projection has been previously discussed by several authors [16–18,23–25]. To determine if this phenomenon is more general, we

TABLE III. Similar to Table. I but for the VAP-JTA calculations. $\langle A\rangle = 8$ is imposed.

$\|\Phi_0\rangle$	$E^*_{\rm JTA}$(MeV)	$E_{\rm TA}$(MeV)	$Q_{\rm TA}$	$\gamma_{\rm TA}(^\circ)$	E_A(MeV)	Q_A	$\gamma_A(^\circ)$	$E_{\rm HFB}$(MeV)	$Q_{\rm HFB}$	$\gamma_{\rm HFB}(^\circ)$	$\langle A\rangle$
1	−86.919	−79.879	19.057	−16.964	−75.600	17.482	−20.225	−73.781	16.230	−23.772	8.000
2	−86.919	−79.879	19.057	−16.963	−75.641	17.510	−20.119	−73.830	16.264	−23.604	8.000
3	−86.919	−79.879	19.057	−16.963	−75.644	17.520	−20.068	−73.845	16.281	−23.506	8.000

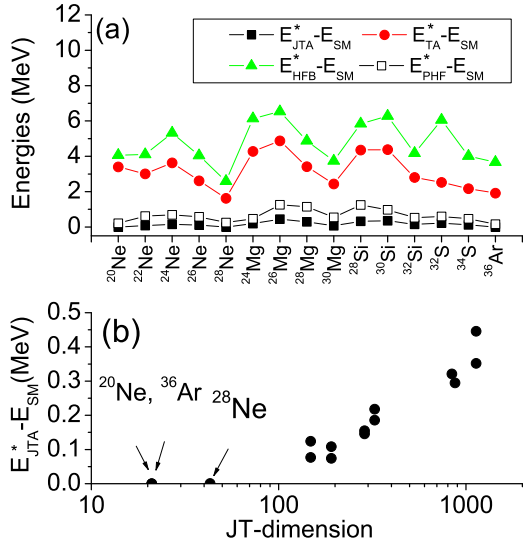

FIG. 1. (Color online) (a) Calculated ground state energies relative to the shell model results, E_{SM}. (b) Relative VAP-JTA energy, $E^*_{JTA} - E_{SM}$, versus the shell model dimension, N_{JT}, in JT subspace.

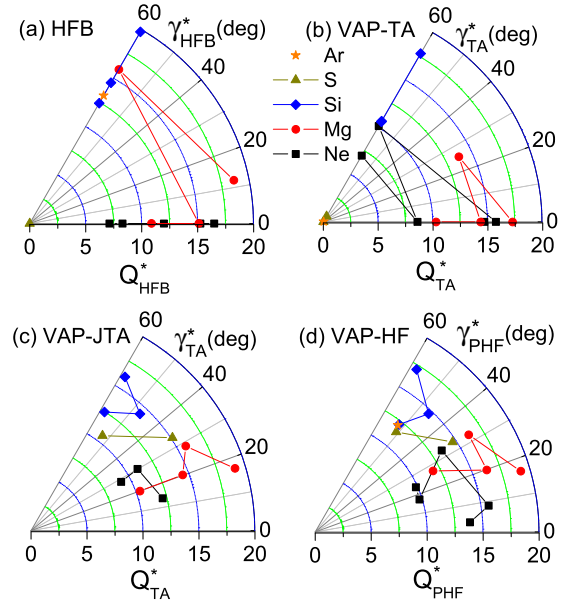

FIG. 2. (Color online) Associated intrinsic quadrupole moments Q and γ for (a) HFB vacuum states, (b) VAP-TA states, (c) VAP-JTA states, and (d) VAP-HF states which is based on a slater determinant.

performed systematic VAP calculations for a larger number of even-even *sd*-shell nuclei.

IV. VAP CALCULATIONS FOR EVEN-EVEN *sd*-SHELL NUCLEI

VAP calculations have been performed for the ground states of even-even *sd*-shell nuclei. The calculated energies relative to the shell model ones are shown in Fig. 1(a). The numerical results are given in Table IV. Here, we did not include the oxygen isotopes and the $N = 20$ isotones because their VAP-JTA energies are exactly the same as the shell model results (E_{SM}). This special case is discussed below. The VAP-JTA energies are much lower than those of HFB and VAP-TA. Moreover, The VAP-JTA energies for ^{20}Ne, ^{28}Ne, and ^{36}Ar nuclei are exactly the same as the shell model results [see also Fig. 1(b)]. This can be understood by comparing the number of VAP parameters, N_{VAP}, with the shell model dimension, N_{JT} (the total number of the independent basis states with good JT). Here, $N_{VAP} = 42$. The N_{JT} values with $J = 0$ and $T = 0$ for both ^{20}Ne and ^{36}Ar are only 21. For ^{28}Ne, N_{JT} for $J = 0$ and $T = 4$ is 43. It looks that when N_{JT} is less than, or close to N_{VAP}, then the VAP-JTA energy is likely to be the same as the shell model one. Indeed, for all even-even oxygen isotopes and for the $N = 20$ isotones, for which $N_{JT} \leqslant N_{VAP}$, we have obtained $E^*_{JTA} = E_{SM}$. In Fig. 1(b), one can also see that the energy difference $E^*_{JTA} - E_{SM}$ increases

TABLE IV. Converged energies and associated shape parameters for even-even *sd*-shell nuclei calculated with the USDB Hamiltonian.

Nucleus			VAP-JTA			VAP-TA			HFB			VAP-HF		
	N_{JT}	E_{SM}	E^*_{JTA}	Q^*_{TA}	γ^*_{TA}	E^*_{TA}	Q^*_{TA}	γ^*_{TA}	E^*_{HFB}	Q^*_{HFB}	γ^*_{HFB}	E^*_{PHF}	Q^*_{PHF}	γ^*_{PHF}
^{20}Ne	21	−40.472	−40.472	–	–	−37.069	14.7	0.0	−36.404	15.3	0.0	−40.265	13.861	3.551
^{22}Ne	148	−57.578	−57.501	12.1	13.8	−54.572	15.8	0.0	−53.474	16.5	0.0	−56.958	15.675	8.632
^{24}Ne	287	−71.725	−71.570	11.0	30.1	−68.084	10.1	60.0	−66.402	12.0	0.0	−71.037	13.449	32.786
^{26}Ne	191	−81.564	−81.465	9.2	28.4	−78.949	8.6	0.0	−77.518	8.3	0.0	−80.988	9.760	17.265
^{28}Ne	43	−86.543	−86.543	–	–	−84.920	7.0	60.0	−83.949	7.1	0.0	−86.294	9.848	23.934
^{24}Mg	325	−87.105	−86.919	19.1	17.0	−82.831	17.3	0.0	−80.965	18.7	12.0	−86.636	19.165	16.427
^{26}Mg	1132	−105.521	−105.075	15.8	28.7	−100.648	13.8	25.7	−98.992	15.9	60.0	−104.264	16.238	32.331
^{28}Mg	874	−120.500	−120.205	14.5	20.2	−117.091	14.4	0.0	−115.625	15.1	0.0	−119.354	16.306	19.835
^{30}Mg	191	−130.474	−130.400	10.4	20.0	−128.035	10.3	0.0	−126.735	10.9	0.0	−129.926	11.864	27.322
^{28}Si	839	−135.860	−135.539	16.1	58.6	−131.501	17.8	60.0	−130.021	19.8	60.0	−134.617	17.116	58.038
^{30}Si	1132	−154.754	−154.402	14.3	47.0	−150.380	10.6	60.0	−148.475	14.5	60.0	−153.777	14.633	46.167
^{32}Si	287	−170.519	−170.373	12.5	58.2	−167.721	10.6	60.0	−166.344	12.4	60.0	−169.996	12.175	52.023
^{32}S	325	−182.452	−182.234	15.1	33.3	−179.925	0.6	60.0	−176.393	0.0	0.0	−181.856	14.681	33.188
^{34}S	148	−202.504	−202.380	10.6	53.0	−200.331	0.0	0.0	−198.493	0.0	0.0	−202.039	11.496	50.992
^{36}Ar	21	−230.277	−230.277	–	–	−228.355	0.0	0.0	−226.611	13.2	60.0	−230.112	12.068	52.293

TABLE V. VAP results with JTA projection for ^{20}Ne.

$\|\Phi_0\rangle$	$E^*_{\rm JTA}$(MeV)	$E_{\rm TA}$(MeV)	$Q_{\rm TA}$	$\gamma_{\rm TA}(^\circ)$
1	−40.472	−28.284	6.314	−45.134
2	−40.472	−30.468	11.873	−124.746
3	−40.472	−27.932	9.876	2.592

with $N_{\rm JT}$. The largest $E^*_{\rm JTA} - E_{\rm SM} = 0.446$ MeV is obtained for ^{26}Mg, corresponding to the largest $N_{\rm JT} = 1132$.

The quadrupole moment and the γ degree of freedom can be extracted using Eqs. (10) and (11). In Fig. 2(a), the $\gamma^*_{\rm HFB}$ values in HFB are either 0° or 60°, except $\gamma^*_{\rm HFB} = 12^\circ$ for ^{24}Mg, thus supporting the conclusion that HFB likely presents axially deformed shapes. In Fig. 2(b), the shapes in VAP-TA calculations still remain axially symmetric, except for ^{26}Mg, which has $\gamma^*_{\rm TA} = 25.7^\circ$. Quite differently, the $\gamma^*_{\rm TA}$ values in the VAP-JTA calculations [Fig. 2(c)] show that all these nuclei are nonaxial without exception. Comparing these results with those of Fig. 2(a), one can conclude that the triaxiality in VAP-JTA is definitely a beyond mean-field effect, which is likely to be a universal phenomenon. Figure 2(b), however, excludes the possibility that the isospin projection and the mass projection lead to triaxiality. Thus, the only possible cause of the triaxiality is the beyond mean-field spin projection.

To study directly the effect of spin projection, one can start from a Hartree-Fock (HF) Slater determinant (SD) and perform VAP calculations with only spin projection (called VAP-HF). The converged energies, $E^*_{\rm PHF}$, relative to $E_{\rm SM}$, are shown in Fig. 1(a). The results show that VAP-HF is better than VAP-TA, and quite close to the VAP-JTA. The quadrupole moment $Q^*_{\rm PHF}$ and $\gamma^*_{\rm PHF}$ corresponding to $E^*_{\rm PHF}$ can be calculated using Eqs. (10) and (11) with $|\Psi\rangle$ replaced by the converged SD. These quantities are uniquely determined, and are shown in Fig. 2(d). Again, all the $\gamma^*_{\rm PHF}$ values are distributed in the interval (0°,60°), which is very similar to Fig. 2(c). Therefore, we could conclude that VAP results that include spin projection can always be associated with intrinsic states having triaxial deformation.

One more interesting phenomenon, however, is related to the VAP-JTA calculations for ^{20}Ne, ^{28}Ne, and ^{36}Ar. We have shown above that the $E^*_{\rm JTA}$ energies of these nuclei are the same as the exact shell model results. Surprisingly, the corresponding $Q_{\rm TA}$ and $\gamma_{\rm TA}$ values are not unique, which is quite different from other nuclei with $E^*_{\rm JTA} > E_{\rm SM}$. For example, the results for ^{20}Ne are shown in Table V. With the same converged $E^*_{\rm JTA} = -40.472$ MeV, one can clearly see that starting with different initial states $|\Phi_0\rangle$, the results for $Q_{\rm TA}$ and $\gamma_{\rm TA}$ could be different. These results indicate that it may not be possible to associate a unique intrinsic deformation with an exact eigenstate of the Hamiltonian.

V. SUMMARY

We implemented an algorithm that performs variation after projection (VAP) on spin, isospin, and mass number of a triaxially deformed Hartree-Fock-Bogoliubov vacuum state. This is the first projected mean field study that includes all these quantum numbers.

We start from a randomly chosen HFB vacuum state and carry out VAP calculations for ^{24}Mg in the sd shell with various projections. In the VAP-A case the converged solution is independent of the Fermi level (chemical potential). Although the associated HFB vacuum does not have definite quadrupole moment $Q_{\rm HFB}$ and triaxial deformation parameter $\gamma_{\rm HFB}$, one can use the unique Q_A and γ_A to describe the intrinsic deformation of the VAP-A state. Similarly, in the VAP-TA calculations, Q_A and γ_A cannot be uniquely determined, but $Q_{\rm TA}$ and $\gamma_{\rm TA}$ are unique and can be associated with the intrinsic deformation of the VAP-TA state. It is not possible to directly define deformation parameters Q and γ for the VAP-JTA wave function, which has the symmetries fully restored, but the $Q_{\rm TA}$ and $\gamma_{\rm TA}$ calculated with the VAP-JTA vacuum state $|\Phi\rangle$ are also unique, and can be associated with the intrinsic deformation of the VAP-JTA state.

Systematical VAP calculations of even-even sd-shell nuclei have been performed using the USDB Hamiltonian. The VAP-JTA energies, $E^*_{\rm JTA}$, are very close to the shell model results, $E_{\rm SM}$. Moreover, the relative energy, $E^*_{\rm JTA} - E_{\rm SM}$, increases with the shell model dimension $N_{\rm JT}$. The shapes described by the HFB minima are always axial. However, with spin projection VAP calculations always produce triaxial shapes. We believe that such triaxiality is an universal phenomenon caused by the beyond mean-field dynamic correlations. Finally, we show that those VAP-JTA states reaching the exact shell model results do not have clearly defined intrinsic shapes.

ACKNOWLEDGMENTS

Z-C.G. thanks Prof. G. F. Bertsch for fruitful discussions, and Prof. Y. Sun for reading the manuscript. This work is partly supported by the National Natural Science Foundation of China under Contract Nos. 11175258, 11575290, 11321064, and 11275068; the CUSTIPEN (China-US Theory Institute for Physics with Exotic Nuclei) under US DOE Grant No. DE-FG02-13ER42025; the Open Project Program of State Key Laboratory of Theoretical Physics, Institute of Theoretical Physics, Chinese Academy of Sciences, China (No. Y5KF141CJ1). M.H. acknowledges the National Science Foundation Grant No. PHY-1404442.

[1] J.-P. Delaroche *et al.*, Phys. Rev. C **81**, 014303 (2010).
[2] I. Maqbool, J. A. Sheikh, P. A. Ganai, and P. Ring, J. Phys. G **38**, 045101 (2011).
[3] R. Rodríguez-Guzmán, Y. Alhassid, and G. F. Bertsch, Phys. Rev. C **77**, 064308 (2008).
[4] L. M. Robledo and G. F. Bertsch, Phys. Rev. C **84**, 014312 (2011).
[5] K. W. Schmid, Prog. Part. Nucl. Phys. **52**, 565 (2004).
[6] B. A. Brown and W. A. Richter, Phys. Rev. C **74**, 034315 (2006).

[7] P. Ring and P. Schuck, *The Nuclear Many-Body Problem* (Springer Verlag, New York/Heidelberg/Berlin, 1980).
[8] P.-G. Reinhard, D. J. Dean, W. Nazarewicz, J. Dobaczewski, J. A. Maruhn, and M. R. Strayer, Phys. Rev. C **60**, 014316 (1999).
[9] R. R. Rodríguez-Guzmán, J. L. Egido, and L. M. Robledo, Phys. Lett. B **474**, 15 (2000); Phys. Rev. C **62**, 054319 (2000).
[10] Zao-Chun Gao, Mihai Horoi, and Y. S. Chen, Phys. Rev. C **80**, 034325 (2009).
[11] D. Liu and J. Nocedal, Mathematical Programming B **45**, 503 (1989).
[12] D. Kurath, Phys. Rev. C **5**, 768 (1972).
[13] W. Koepf and P. Ring, Phys. Lett. B **212**, 397 (1988).
[14] P. Bonche, H. Flocard, and P. H. Heenen, Nucl. Phys. A **467**, 115 (1987).
[15] R. K. Sheline, I. Ragnarsson, S. Åberg, and A. Watts, J. Phys. G **14**, 1201 (1988).
[16] Michael Bender and Paul-Henri Heenen, Phys. Rev. C **78**, 024309 (2008).
[17] J. M. Yao, J. Meng, P. Ring, and D. Vretenar, Phys. Rev. C **81**, 044311 (2010).
[18] Tomás R. Rodríguez and J. L. Egido, Phys. Rev. C **81**, 064323 (2010).
[19] Z.-C. Gao, Q.-L. Hu, and Y. S. Chen, Phys. Lett. B **732**, 360 (2014).
[20] Q.-L. Hu, Z.-C. Gao, and Y. S. Chen, Phys. Lett. B **734**, 162 (2014).
[21] L.-J. Wang, F.-Q. Chen, T. Mizusaki, M. Oi, and Y. Sun, Phys. Rev. C **90**, 011303(R) (2014).
[22] K. Hara and Y. Sun, Int. J. Mod. Phys. E **4**, 637 (1995).
[23] A. Hayashi, K. Hara, and P. Ring, Phys. Rev. Lett. **53**, 337 (1984).
[24] K. Enami, K. Tanabe, N. Yoshinaga, and K. Higashiyama, Prog. Theor. Phys. **104**, 757 (2000).
[25] J. M. Yao, J. Meng, P. Ring, and D. Pena Arteaga, Phys. Rev. C **79**, 044312 (2009).